China Ocean Engineering, Vol.21, No.1, pp.91 – 104

Analysis of Responses of Floating Dual Pontoon Structure

WENG Wen-Kai (翁文凯)[1] and CHOU Chung-Ren (周宗仁)

Department of Harbor and River Engineering, National Taiwan Ocean University, Keelung 20229, Taiwan, China

(Received 18 November 2005; received revised form 20 September 2006; accepted 29 October 2006)

ABSTRACT

A numerical model is developed by use of the boundary integral equation method to investigate the responses of a two-dimensional floating structure. The structure under consideration consisting of two pontoons, is connected by a rigid framework, and linked to the sea floor by a mooring system. The theoretical conception is based on potential theory with linear external forces, and applied to an arbitrarily shaped body and water depth. The discussion includes the influence of draft and space between pontoons on the responses of the floating structure. Finally, the validity of the method is adequately verified by experimental results.

Key words: *boundary element method*; *floating structure*; *dual pontoon*

1. Introduction

Floating structures are increasingly used in the nearshore regions to prevent wave energy or control shoreline erosion. Owing to the various types and the advantage of easy installation, floating structures offer engineers another choice to design a suitable or relatively inexpensive structure for local environment (e.g. weak foundation, large tide range) or special requirements (e.g. aesthetic, water circulation and ecological considerations). Though floating structures have many excellences in environmental improvement, they are often preferred in relatively low wave energy regions.

Many discussions concerning the characteristics and efficiency of floating structures have been made, not only in various analytic theories but also in the improvement of structure type, by many authors in recent years. Some researchers, e.g., Leonard *et al*. (1983), discussed the hydrodynamic interference between floating cylinders in oblique sea by taking advantage of finite element method. McIver (1986) used the method of matched eigenfunction expansions to investigate interaction effects due to waves incident upon an adjacent floating bridge. Wang *et al*. (2006) showed the dynamic behavior of a pontoon-separated floating bridge by means of finite element method. Drimer *et al*. (1992) presented a simplified analytical model for a floating breakwater in finite water depth. Sannasiraj *et al*. (1998) utilized two-dimensional finite element methods to analyze the mooring forces and responses of a single floating pontoon-type breakwater. On the other hand, some researchers were devoted to the development of the forms of floating structures and the investigation of the efficiency of structures. McCartney (1985) classified floating breakwaters into four categories. Discussions including advantages and disadvantages of structures, mooring system, anchorage methods, etc., were presented in detail in

1 Corresponding author. E-mail: wkweng@mail.ntou.edu.tw

that paper. Isaacson and Byres (1988) showed the responses of a floating breakwater and compared the results with experimental and field data. Murali and Mani (1997) discussed the reflection and transmission characteristics of cage floating breakwaters in an experimental manner.

A numerical model is developed for analyzing the behaviors of a floating structure by use of boundary element method in this paper. The structure comprising two arbitrarily shaped pontoons is connected by a rigid framework and linked to the seabed by a linear mooring system. Theoretical analysis is based on potential theory with linear conditions, and both scattering and radiating waves are discussed in the analytic process. A model test is carried out in a water tank to verify the numerical results. Finally, the influences of each pontoon's dimensions and clear distance between pontoons on its responses are discussed.

2. Theoretical Formulas

The definition sketch of the analyzed region is shown in Fig. 1. A floating structure consists of two pontoons and is sited on a sea. Cartesian coordinates are employed and the z-axis is directed vertically upwards from its origin on the undisturbed free surface. The structure is located symmetrically at $x = 0$. Each pontoon is linked to the sea floor by an idealized mooring system. The motions of the structure are assumed to be small and linear when the structure is subjected to a train of small amplitude waves of height ζ_0 and frequency σ traveling in the negative x-direction. The fluid in the analyzed region are assumed to be inviscid and incompressible. On the above assumptions, the motion of fluid will be irrotational and can be described in terms of velocity potential $\Phi(x, z; t) = (g\zeta_0/\sigma)\phi(x, z)e^{i\sigma t}$, and the potential of the analyzed region must satisfy Laplace's equation.

$$\nabla^2\phi(x, z) = 0. \tag{1}$$

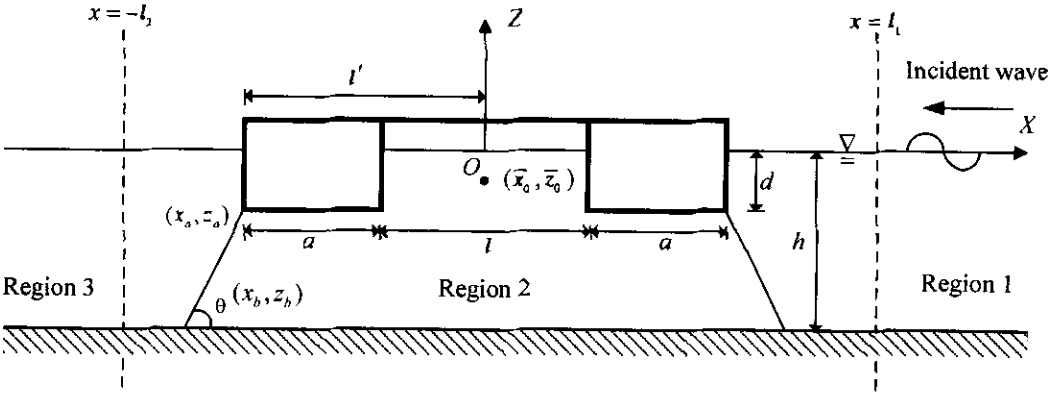

Fig. 1. Definition sketch.

The analyzed region will be further divided into three sub-regions to simplify the problem. Those sub-regions are termed as region 1 ($x \geqslant l_1$), region 2 ($-l_2 \leqslant x \leqslant l_1$) and region 3 ($x \leqslant -l_2$), and their complex potentials denoted by ϕ_j ($j = 1, 2, 3$). Region 2 includes the floating structure; the fluid motion within this region will contain scattering and radiating effect. Regions 1 and 3 are set at the

positions far away from the structure and are assumed to be beyond the disturbance caused by floating structure's motions.

2.1 Potential of Regions 1 and 3

The potential of regions 1 and 3 can be described in the following form, respectively,

$$\phi_1(x,z) = \left[e^{ik(x-l_1)} + K_r e^{ik(x+l_1)} \right] \frac{\cosh k(h+z)}{\cosh kh}, \tag{2}$$

$$\phi_3(x,z) = K_t e^{-ik(x+l_2)} \frac{\cosh k(h+z)}{\cosh kh}, \tag{3}$$

where, K_r and K_t, in complex forms, are coefficient of reflection and transmission, respectively; k is the incident wave number, which is the root of the linear dispersion relation $\sigma^2 = gk \tanh kh$. The potential of regions 1 and 3, together with its normal derivative at auxiliary boundaries $x = l_1$ and $x = -l_2$ can be expressed by:

$$\phi_1(l_1,z) = (1 + K_r) \frac{\cosh k(h+z)}{\cosh kh}; \tag{4}$$

$$\bar{\phi}_1(l_1,z) = ik(1 - K_r) \frac{\cosh k(h+z)}{\cosh kh}; \tag{5}$$

$$\phi_3(-l_2,z) = K_t \frac{\cosh k(h+z)}{\cosh kh}; \tag{6}$$

$$\bar{\phi}_3(-l_2,z) = -ikK_t \frac{\cosh k(h+z)}{\cosh kh}. \tag{7}$$

2.2 Boundary Conditions of Region 2

Region 2 is enclosed by the free surface S_f, the immersed structure surface S_b, the impermeable sea floor surface S_s and two fictitious boundaries S_1 and S_2. The boundary conditions on the free surface and sea floor are subject to the following equations, respectively,

$$\frac{\partial \phi}{\partial z} = \frac{\sigma^2}{g}\phi \qquad \text{on} \quad z = 0; \tag{8}$$

$$\frac{\partial \phi}{\partial z} = 0 \qquad \text{on} \quad z = -h. \tag{9}$$

The requirements of continuity of mass and energy flux across the fluid interfaces between each region imply the following matching conditions:

$$\phi_1 = \phi_2 \qquad \text{on} \quad x = l_1; \tag{10}$$

$$\frac{\partial \phi_1}{\partial x} = \frac{\partial \phi_2}{\partial x} \qquad \text{on} \quad x = l_1; \tag{11}$$

$$\phi_2 = \phi_3 \qquad \text{on} \quad x = -l_2; \tag{12}$$

$$\frac{\partial \phi_2}{\partial x} = \frac{\partial \phi_3}{\partial x} \qquad \text{on} \quad x = -l_2. \tag{13}$$

For the analysis of structure responses, it is assumed that the structure behaves as a two-dimensional rigid body, and the structure will undergo small amplitude surge, heave and pitch motions when it is in response to the incident and diffracted waves. The displacement for those three mode motions may then be expressed as:

$$x_0 - \bar{x}_0 = \xi e^{i\sigma t},\ z_0 - \bar{z}_0 = \eta e^{i\sigma t},\ \delta = \omega e^{i\sigma t}, \tag{14}$$

in which, $(\bar{x}_0, \bar{z}_0)$ is the coordinate of the center of mass of the structure at rest and (x_0, z_0) is its instantaneous position; ξ, η and ω are amplitude of surge, heave and pitch motions, respectively. The first order kinematic boundary on the immersed surface of the structure may then be written as:

$$\frac{\partial \Phi_b}{\partial n} = \frac{\partial (x_0 - \bar{x}_0)}{\partial t}\frac{\partial x}{\partial n} + \frac{\partial (z_0 - \bar{z}_0)}{\partial t}\frac{\partial z}{\partial n} + \frac{\partial \delta}{\partial t}\left[\frac{\partial x}{\partial n}(z - \bar{z}_0) - \frac{\partial z}{\partial n}(x - \bar{x}_0)\right]. \tag{15}$$

The equations of motion of the structure under fluid pressure and external forces may be expressed as:

$$\begin{cases} m\dfrac{d^2(x_0 - \bar{x}_0)}{dt^2} = \displaystyle\int_{S_b} P\frac{\partial x}{\partial n}ds + \sum_{j=1}^{n}\hat{F}_x^j \\ m\dfrac{d^2(z_0 - \bar{z}_0)}{dt^2} = \displaystyle\int_{S_b} P\frac{\partial z}{\partial n}ds + R_z + \sum_{j=1}^{n}\hat{F}_z^j \\ I_y\dfrac{d^2\delta}{dt^2} = \displaystyle\int_{S_b} P\left[\frac{\partial x}{\partial n}(z - \bar{z}_0) - \frac{\partial z}{\partial n}(x - \bar{x}_0)\right]ds + M_y + \sum_{j=1}^{n}\hat{M}_y^j \end{cases} \tag{16}$$

where, m is the mass of the structure, I_y the mass moment of inertia about the center of mass of the structure, P the dynamic pressure of the fluid, R_z and M_y are restoring force and moment, and $\hat{F}_x$, $\hat{F}_z$ and $\hat{M}_y$ are forces and moments acting upon the structure due to each mooring lines. The foregoing pressure of the fluid and restoring components are given by

$$\begin{cases} P = -\rho\dfrac{\partial \Phi}{\partial t} = -i\rho g\zeta_0\phi e^{i\sigma t} \\ R_z = -\displaystyle\int_{S_b}\rho g(z_0 - \bar{z}_0)\frac{\partial z}{\partial n}ds \\ M_y = -\displaystyle\int_{S_b}\rho g\delta(x_0 - \bar{x}_0)\left[\frac{\partial x}{\partial n}(z - \bar{z}_0) - \frac{\partial z}{\partial n}(x - \bar{x}_0)\right]ds \end{cases} \tag{17}$$

The mooring forces and moments, $\hat{F}_x$, $\hat{F}_z$, and $\hat{M}_y$, are caused by the linear system, like spring, as shown in Fig. 1. Considering the j-th mooring line AB, with its spring constant K^j and pretension F_0, the coordinates of attachment point on the structure and on the sea floor are (x_a, z_a) and (x_b, z_b), respectively. Ignoring the inertia effects of the mooring line and the viscous forces on the line, each component of forces and moments due to this mooring line can be expressed as:

$$\begin{cases} \hat{F}_x^j = -K_{xx}^j(x_0 - \bar{x}_0) - K_{xz}^j(z_0 - \bar{z}_0) - K_{x\delta}^j\delta \\ \hat{F}_z^j = -K_{zx}^j(x_0 - \bar{x}_0) - K_{zz}^j(z_0 - \bar{z}_0) - K_{z\delta}^j\delta \\ \hat{M}_y^j = -K_{\delta x}^j(x_0 - \bar{x}_0) - K_{\delta z}^j(z_0 - \bar{z}_0) - K_{\delta\delta}^j\delta \end{cases} \tag{18}$$

where,

$$K_{xx}^j = \frac{(x_b - x_a)^2}{l_{ab}^2}K^j + \frac{(z_b - z_a)^2}{l_{ab}^2}\frac{F_0}{l_{ab}};$$

$$K_{zz}^{j} = \frac{(z_b - z_a)^2}{l_{ab}^2} K^j + \frac{(x_b - x_a)^2}{l_{ab}^2} \frac{F_0}{l_{ab}};$$

$$K_{xz}^{j} = K_{zx}^{j} = \frac{(x_b - x_a)(z_b - z_a)}{l_{ab}^2} \left(K^j - \frac{F_0}{l_{ab}} \right);$$

$$K_{x\delta}^{j} = K_{\delta x}^{j} = \frac{(x_b - x_a)}{l_{ab}^2} \left[(z_b - z_a)(x_a - \bar{x}_0) - (x_b - x_a)(z_a - \bar{z}_0) \right] K^j + \frac{(z_b - z_a)}{l_{ab}^2} \left[(x_b - x_a)(x_a - \bar{x}_0) - (z_b - z_a)(z_a - \bar{z}_0) \right] \frac{F_0}{l_{ab}};$$

$$K_{z\delta}^{j} = K_{\delta z}^{j} = \frac{(z_b - z_a)}{l_{ab}^2} \left[(z_b - z_a)(x_a - \bar{x}_0) - (x_b - x_a)(z_a - \bar{z}_0) \right] K^j + \frac{(x_b - x_a)}{l_{ab}^2} \left[(x_b - x_a)(x_a - \bar{x}_0) + (z_b - z_a)(z_a - \bar{z}_0) \right] \frac{F_0}{l_{ab}};$$

$$K_{\delta\delta}^{j} = \frac{\left[(x_b - x_a)(z_a - \bar{z}_0) - (z_b - z_a)(x_a - \bar{x}_0) \right]^2}{l_{ab}^2} K^j + \frac{\left[(z_b - z_a)(z_a - \bar{z}_0) + (x_b - x_a)(x_a - \bar{x}_0) \right]}{l_{ab}^2} \frac{F_0}{l_{ab}} + \frac{\left[(z_b - z_a)(z_a - \bar{z}_0) + (x_b - x_a)(x_a - \bar{x}_0) \right]}{l_{ab}} F_0;$$

$$l_{ab} = \sqrt{(x_b - x_a)^2 + (z_b - z_a)^2}.$$

3. Development of the Theory

The above problem for the fluid potential of region 2 is solved numerically by use of the boundary integral equation method. According to Green's second identity law, the potential of any point on the boundaries of region 2 is subject to the potential on the boundaries together with its first normal derivative. It is written as:

$$\phi(x', z') = \frac{1}{\pi} \int_{\Gamma_2} \left[\frac{\partial \phi(x, z)}{\partial n} ln \frac{1}{r} - \phi(x, z) \frac{\partial}{\partial n} \left(ln \frac{1}{r} \right) \right] \mathrm{d}s \tag{19}$$

where $ln \frac{1}{r}$ is the solution of Laplace equation. When the boundaries enclosing region 2 are partitioned into N segments, Eq. (19) has the following matrix form:

$$\{\phi_i\} = [O_{ij}] \left\{ \frac{\partial \phi}{\partial n_j} \right\} \quad (i, j = 1, 2, \cdots N). \tag{20}$$

3.1 Coefficients of Reflection and Transmission

The coefficient of reflection and transmission can be acquired by use of continuity of mass and energy flux on the fictitious boundaries. Substituting Eq. (5) into Eq. (11), multiplying the result with $\cosh k(h + z)$, and integrating from $z = -h$ to $z = 0$, one has the reflection coefficient, K_r, in terms of the normal derivatives of potential $\bar{\phi}_1$, as:

$$K_r = 1 + \frac{\mathrm{i}}{N_O \sinh kh}\int_{-h}^{0} \bar{\phi}_1 \cosh k(h+z)\,\mathrm{d}z, \quad \text{on} \quad x = l_1, \tag{21}$$

where $N_O = [1 + 2kh/\sinh 2kh]/2$.

Substituting Eq. (21) into Eq. (4), associating the result with Eq. (10), one can write the relation between the potential of the auxiliary boundary, $x = l_1$, and its normal derivative as:

$$\phi(l_1, z) = 2\frac{\cosh k(h+z)}{\cosh kh} + 2\mathrm{i}\frac{\cosh k(h+z)}{N_O \sinh 2kh}\int_{S_1} \bar{\phi}(l_1, z)\cosh k(h+z)\,\mathrm{d}s. \tag{22}$$

Similarly, the coefficient of transmission can be obtained by way of substituting Eq. (7) into Eq. (13), multiplying the result with $\cosh k(h+z)$, and integrating from $z = -h$ to $z = 0$. It has the following form:

$$K_t = \frac{\mathrm{i}}{N_O \sinh kh}\int_{-h}^{0} \bar{\phi}_2 \cosh k(h+z)\,\mathrm{d}z, \quad \text{on} \quad x = -l_2. \tag{23}$$

The relation between potential with its normal derivative on the auxiliary boundary, $x = -l_2$, can also be obtained through substituting Eq. (23) into Eq. (6), associating the result with Eq. (12), and is expressed as:

$$\phi(-l_2, z) = 2\mathrm{i}\frac{\cosh k(h+z)}{N_O \sinh 2kh}\int_{S_2} \bar{\phi}(-l_2, z)\cosh k(h+z)\,\mathrm{d}s. \tag{24}$$

3.2 Motions of Structure

Responses of a floating structure are not only affected by hydrodynamic forces of fluid, induced from scattering and radiating waves, but by the effects of the mooring system. For simplicity, the mooring system is taken to be symmetric fore and aft of the structure. Some terms of mooring forces influencing the motions of the structure will be canceled out, and Eq. (16) can then be simplified to a simpler form. The motion amplitude of the structure can be obtained after arranging Eq. (16), in terms of the potential ϕ_b on the immersed surface of structure, as:

$$\xi/\zeta_0 = \frac{-\mathrm{i}}{c_1 c_4 - c_2 c_3}\left\{c_4\int_{S_b}\phi_b\frac{\partial x}{\partial n}\mathrm{d}s - c_2\int_{S_b}\phi_b\left[\frac{\partial x}{\partial n}(z - \bar{z}_0) - \frac{\partial z}{\partial n}(x - \bar{x}_0)\right]\mathrm{d}s\right\} \tag{25a}$$

$$\eta/\zeta_0 = \frac{-\mathrm{i}}{c_5}\int_{S_b}\phi_b\frac{\partial z}{\partial n}\mathrm{d}s \tag{25b}$$

$$\omega/\zeta_0 = \frac{-\mathrm{i}}{c_1 c_4 - c_2 c_3}\left\{-c_3\int_{S_b}\phi_b\frac{\partial x}{\partial n}\mathrm{d}s + c_1\int_{S_b}\phi_b\left[\frac{\partial x}{\partial n}(z - \bar{z}_0) - \frac{\partial z}{\partial n}(x - \bar{x}_0)\right]\mathrm{d}s\right\} \tag{25c}$$

where,

$$\begin{aligned}
c_1 &= 2\frac{K_{xx}}{\rho g} - \frac{m}{\rho}\frac{\sigma^2}{g}\\
c_2 &= 2\frac{K_{x\delta}}{\rho g} = c_3 = 2\frac{K_{\delta x}}{\rho g}\\
c_4 &= 2\frac{K_{\delta\delta}}{\rho g} + \int_{S_b}(x - \bar{x}_0)\left[\frac{\partial x}{\partial n}(z - \bar{z}_0) - \frac{\partial z}{\partial n}(x - \bar{x}_0)\right]\mathrm{d}s - \frac{I_y}{\rho}\frac{\sigma^2}{g}\\
c_5 &= 2\frac{K_{zz}}{\rho g} + \int_{S_b}\frac{\partial z}{\partial n}\mathrm{d}s - \frac{m}{\rho}\frac{\sigma^2}{g}
\end{aligned} \tag{26}$$

Eqs. (25a) ~ (25c) are the amplitude of surge, heave, pitch motions of the structure, respectively. Substituting Eqs. (25a) ~ (25c) into Eq. (15), associating the result with Eqs. (14a) ~ (14c), the potential on immersed surface of structure can be written as:

$$\frac{\partial \phi_b}{\partial n} = \frac{\sigma^2}{g}\left\{\frac{c_4}{c_1c_4 - c_2c_3}\frac{\partial x}{\partial n}\int_{S_b}\phi_b\frac{\partial x}{\partial n}\mathrm{d}s - \frac{c_2}{c_1c_4 - c_2c_3}\frac{\partial x}{\partial n}\int_{S_b}\phi_b\left[\frac{\partial x}{\partial n}(z-\bar{z}_0) - \frac{\partial z}{\partial n}(x-\bar{x}_0)\right]\mathrm{d}s + \frac{1}{c_5}\frac{\partial z}{\partial n}\int_{S_b}\phi_b\frac{\partial z}{\partial n}\mathrm{d}s - \frac{c_3}{c_1c_4 - c_2c_3}\left[\frac{\partial x}{\partial n}(z-\bar{z}_0) - \frac{\partial z}{\partial n}(x-\bar{x}_0)\right]\int_{S_b}\phi_b\frac{\partial x}{\partial n}\mathrm{d}s + \frac{c_1}{c_1c_4 - c_2c_3}\left[\frac{\partial x}{\partial n}(z-\bar{z}_0) - \frac{\partial z}{\partial n}(x-\bar{x}_0)\right]\int_{S_b}\phi_b\left[\frac{\partial x}{\partial n}(z-\bar{z}_0) - \frac{\partial z}{\partial n}(x-\bar{x}_0)\right]\mathrm{d}s\right\}. \tag{27}$$

By substituting Eqs. (8), (9), (22), (24) and Eq. (27) into Eq. (20), one can obtain the potential and its normal derivative on the boundaries of region 2. The motion amplitude of each mode can be obtained also by means of substituting the potential on the immersed surface of the structure into Eqs. (25a) ~ (25c).

3.3 Forces on Mooring Lines

For a mooring line AB in Fig. 1, its coordinate of attachment point on the structure is transferred from (x_a, z_a) to (x_a', z_a') when the structure oscillates in response to fluid forces. The forces on the mooring line can be estimated easily from lengthening ε and spring constant K_{ab} of mooring line AB, when mooring lines are treated as a linear system, and is expressed as:

$$\frac{F_{ab}}{K_{ab}\zeta_0} = \frac{-1}{l_{ab}}\left\{(x_b - x_a)\frac{(x_0 - \bar{x}_0)}{\zeta_0} + (z_b - z_a)\frac{(z_0 - \bar{z}_0)}{\zeta_0} + [(x_b - x_a)(z_a - \bar{z}_0) - (z_b - z_a)(x_a - \bar{x}_0)]\frac{\delta}{\zeta_0}\right\}. \tag{28}$$

4. Results and Discussions

4.1 Comparison of Numerical and Experimental Results

A wave tank of 50 m in length and 1.2 m in width was used for a series of experiments for verification of the numerical results. Water depth h was maintained at a constant 0.5 meter during the model test. A floating structure model with each rectangular pontoon width a = 25 cm, draft d = 15 cm and clear distance between pontoons l = 50 cm was sited in the wave tank for the experiment. The length of test model was 117 cm in its axis direction (Y axis). Therefore, each gap between the model edge and tank wall under consideration was about 1.5 cm. The other characteristics of the test model were: weight = 76.05 kg, mass moment of inertia I_y = 9.82 kg·m^2, and position of the center of mass under free surface $\bar{z}_0$ = −12.1 cm. For simulation of the mooring system, four taut springs were applied to moor the model; each spring had a spring stiffness K = 0.275 kg/cm in the linear region, and an angle of inclination 54.5° to the horizontal axis. All the above parameters of the model were normal-

ized for the necessary input data of numerical computation, and were given as stiffness $K/(\rho gh) = 0.094$, pretension of each mooring line $F_0/(\rho gh^2) = 0.0246$, mass of structure $m/(\rho gh^2) = 0.26$, mass moment of inertia $I_y/(\rho gh^4) = 0.157$, and dimensions of structure $a/h = 0.5$, $d/h = 0.3$, $l/h = 1.0$, and $\bar{z}_0/h = -0.242$, respectively.

Three-mode displacements of the floating structure and the reflection coefficients induced by the structure were investigated during the model test. The reflection coefficients were obtained by means of the analytic method of Goda and Suzuki (1976). Acceleration transducers and angle sensors were mounded on the structure for measuring displacements of the structure. The position of sensors is generally unable to consist with the center of mass of the model. Therefore, the data from the sensors need to be arranged again through coordinate transformation.

Figs. 2 ~ 4 illustrate the amplitude of three-mode motions of the structure modulating in dimensionless wave period $\sigma^2 h/g$ from the experiment and numerical calculation, respectively. Essentially, the dimensionless amplitude of surge motion decreases monotonously when the wave period shortens; pitch motion has a peak value at the higher frequency $\sigma^2 h/g \approx 2.45$. As regards the heave motion, its amplitude decreases gradually when the incoming wave period $\sigma^2 h/g$ is less than 1.3, but it has a peak value at $\sigma^2 h/g \approx 2.3$. The results of reflection coefficient are shown in Fig. 5, and it generally has an excellent performance in wave attenuation when the structure is affected by incoming waves with a shorter period.

On the whole, most experimental results are in sufficient correlation with numerical analysis results, as observed from the comparisons. The prominent capability of dispersing wave energies and structure motions is therefore confirmed here as being able to be validly predicted. However, the predicted results of heave motion are apparently larger than the experimental results at its peak frequency. It is believed that those differences may be induced by viscosity effects of fluid and energy losses from the gap between the model and water tank.

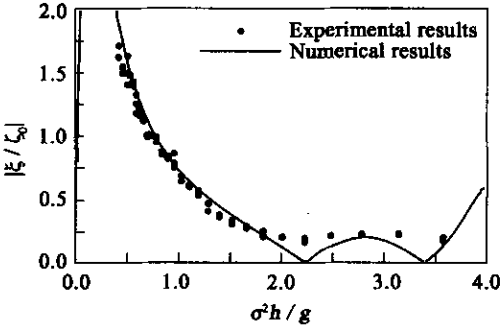

Fig. 2. Comparison between numerical and experimental results for surge motion. ($a/h = 0.5$; $d/h = 0.3$; $l/h = 1.0$; $\theta = 54.5°$)

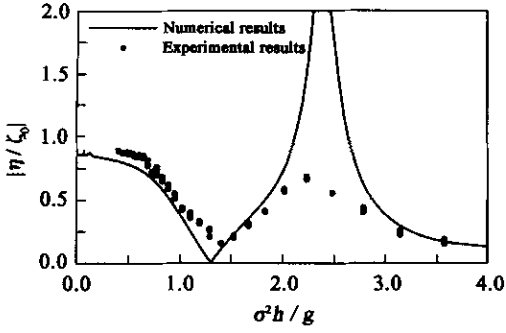

Fig. 3. Comparison between numerical and experimental results for heave motion. ($a/h = 0.5$; $d/h = 0.3$; $l/h = 1.0$; $\theta = 54.5°$)

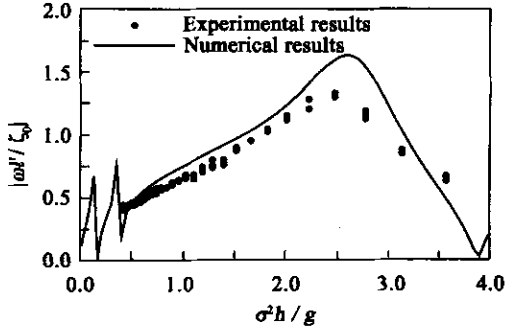

Fig. 4. Comparison between numerical and experimental results for pitch motion. ($a/h = 0.5$; $d/h = 0.3$; $l/h = 1.0$; $\theta = 54.5°$)

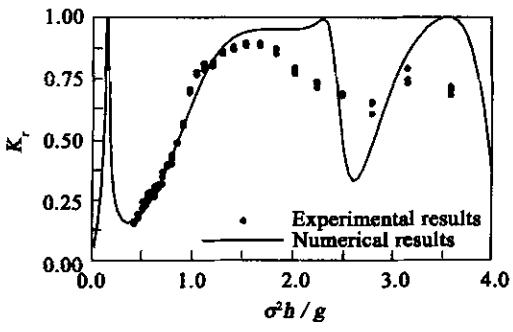

Fig. 5. Comparison between numerical and experimental results for reflection coefficient. ($a/h = 0.5$; $d/h = 0.3$; $l/h = 1.0$; $\theta = 54.5°$)

4.2 Influence of Space Between Pontoons on Motions of Structure

The influences of space, l, between pontoons on the motions of a floating structure are discussed here. A structure composed of two pontoons and having its center of mass $\bar{z}_0 = -0.5d$ is symmetrically sited on the sea. Each pontoon of width $a = 0.25h$ and draft $d = 0.25h$ is ideally assumed to be homogeneous; the mass and mass moment of inertia of the structure will therefore be calculated by a presumed form expressed as $m = 2\upsilon_1\rho ad$, and $I_y = \frac{1}{2}\upsilon_2\rho ad\left[\frac{1}{3}d^2 + \frac{1}{3}a^2 + (a+l)^2\right]$, respectively. Coefficients υ_1 and υ_2 are dependent on the density and shape of the structure, and are simply given the same constant value 0.9 in here. Having the stiffness $K/(\rho gh) = 0.03$ and the angle of inclination $\theta = 60°$, each spring is moored on the edge of pontoon bottom. Pretension of each spring will be given as $F_0/(\rho gh^2) = [2ad/h^2 - m/(\rho h^2)]/(2\sin\theta)$.

Fig. 6 illustrates the variations of surge motion with a dimensionless period $\sigma^2 h/g$ for various spaces of pontoons. The figure demonstrates that the amplitude of surge motion decreases monotonously with shortening wave period, until the amplitude reaches a small value.

Fig. 7 shows the results for heave motion. The dimensionless amplitude of heave motion will approach to a constant value when the structure is affected by a longer period wave, and then will have a monotonic decrease with the shortening wavelength. Besides, heave motion in the ranges analyzed has a peak response which appears in a higher frequency range except for the case of small space between pontoons $l = 0.1h$. It has a tendency that a longer space between pontoons will lead to a lower frequency of peak response. Those phenomena are different from the behavior of single floating bodies and it is believed that those variations are caused by the space between pontoons.

The influences of space between pontoons on pitch motion are shown in Fig. 8. As can be seen, the peak frequency of pitch motion trends down as the space between pontoons increases gradually, and the value of peak response also decays. The main reason is that a longer space will give the structure a larger mass moment of inertia and a larger restoring moment.

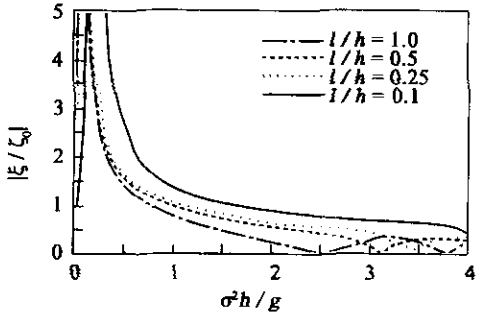

Fig. 6. Influence of space between pontoons on surge motion.
($a/h = d/h = 0.25$; $K/(\rho gh) = 0.03$; $\theta = 60°$)

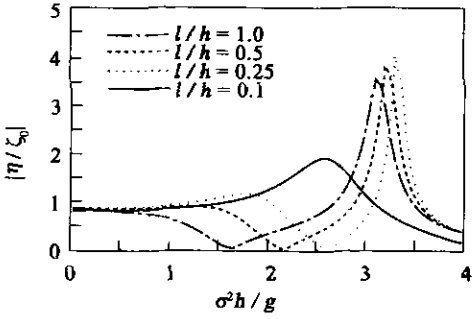

Fig. 7. Influence of space between pontoons on heave motion.
($a/h = d/h = 0.25$; $K/(\rho gh) = 0.03$; $\theta = 60°$)

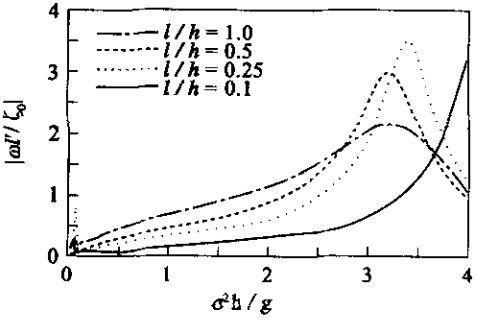

Fig. 8. Influence of space between pontoons on pitch motion.
($a/h = d/h = 0.25$; $K/(\rho gh) = 0.03$; $\theta = 60°$)

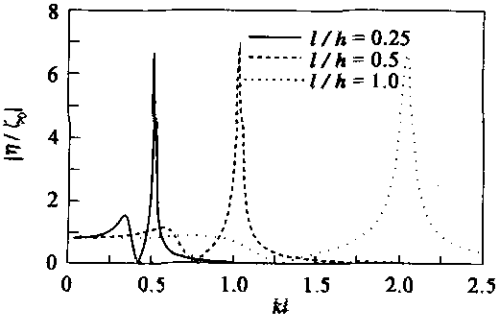

Fig. 9. Relation between peak responses of heave motion and space.
($a/h = 0.25$; $d/h = 0.5$; $K/(\rho gh) = 0.05$; $\theta = 30°$)

According to the above results, the space has a great effect upon the structure 's motions; it not only changes the peak frequency of pitch motion, but induces a peak response of heave motion at a high frequency. Those peak frequencies of heave motion will have a correlation between each other, if floating structures are under the same conditions but with different spaces between pontoons. Fig. 9 illustrates the relations between heave motions and parameter kl for three cases $l/h = 0.25$, 0.5 and 1.0. The conditions of the structure are: width $a = 0.25h$, draft $d = 0.5h$ of each pontoon and center of mass $\bar{z}_0 = -0.5d$. The stiffness of the mooring line and its angle of inclination are $K/(\rho gh) = 0.05$ and $\theta = 30°$, respectively. As can be seen, heave motion has its peak response located at $kl = 2.0472$, 1.0282 and 0.514 for $l/h = 1.0$, 0.5 and 0.25. The kl of peak response is found to have linear relation to space of pontoons l/h. For the case $l/h = 1.0$, the kl of peak response is twice of case $l/h = 0.5$, and is four times of the case $l/h = 0.25$. The results for another case, $a = d = 0.5h$, $K/(\rho gh) = 0.06$ and $\theta = 90°$ (i.e. tension leg type), are shown in Fig. 10. It also displays the same relations as described above notwithstanding the frequencies of peak responses are different

from each other. Obviously, parameter kl is a very important factor for the peak response of heave motion, and the understanding of its influence will be useful for the applications of this kind of floating structures.

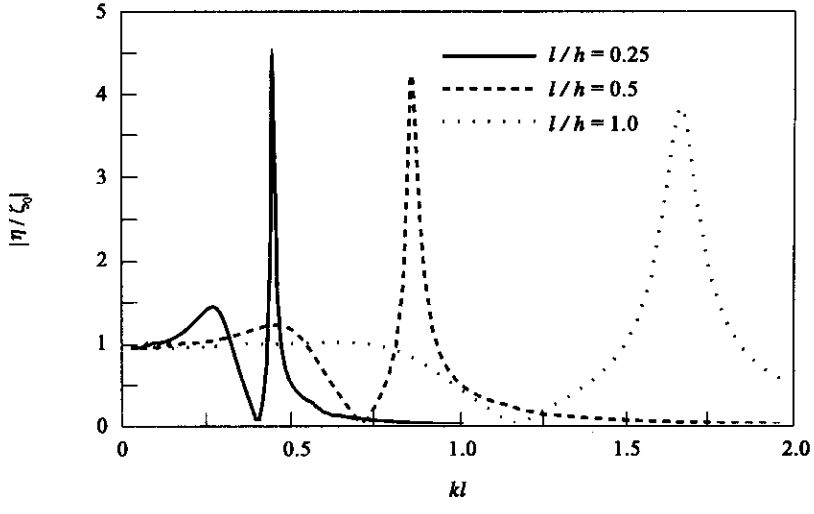

Fig. 10. Relation between peak responses of heave motion and space. ($a/h = d/h = 0.5$; $K/(\rho gh) = 0.06$; $\theta = 90°$)

4.3 Influences of Pontoon Dimension on Motions of Structure

The influences of pontoon dimension on the motions of the structure are shown in Figs. 11 ~ 13 for pontoon draft $d/h = 0.25$, 0.375 and 0.5. In those cases, all structure parameters, including pontoon width, distance between pontoons, stiffness and angle of inclination of mooring lines, are kept constant expect for the center of mass of the structure. The coordinate of the center of mass in the above cases is similarly taken as $\bar{z}_0 = -0.5d$, and it changes with the pontoon draft.

Figs. 11 ~ 13 illustrate the normalized amplitude of three mode motions, surge, pitch and heave, as a function of dimensionless period $\sigma^2 h/g$, respectively. The variations of surge motion, as can be seen from Fig. 11, do not have a large difference when the pontoon draft is changed. The peak frequency of pitch motion, as shown in Fig. 12, obviously has a tendency towards longer period as pontoon draft is increased. It can be understood that the floating structure with a larger draft will cause a larger mass moment of inertia and will induce a lower frequency of peak response. Although the characteristic of structure's motions in surge and pitch mode is obvious and comprehensible, it is still difficult to distinguish between the variations of a dual pontoon structure and a single floating body when one observes those two mode motions from Figs. 11 and 12.

The results for heave motion, as shown in Fig. 13, are similar to the behavior of a single floating body in low frequency range, but they often have a peak response in high frequency range. The frequency of peak response also has a tendency to decrease when the pontoon draft increases, implying that the peak response of heave motion at high frequency is subject not only to the space between pon-

toons, but to the forces of the mooring system, hydrodynamic buoyancy, mass of the structure, etc.

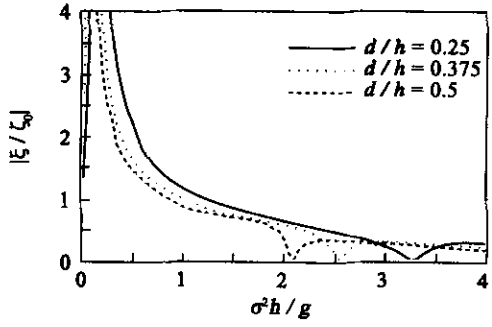

Fig. 11. The influence of pontoon draft on surge motion.
($a/h = d/h = 0.25$; $K/(\rho gh) = 0.05$; $l/h = 0.5$; $\theta = 45°$)

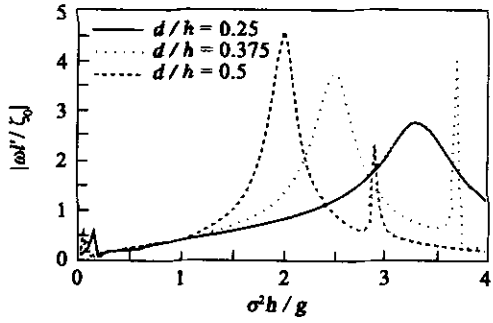

Fig. 12. The influence of pontoon draft on pitch motion.
($a/h = d/h = 0.25$; $K/(\rho gh) = 0.05$; $l/h = 0.5$; $\theta = 45°$)

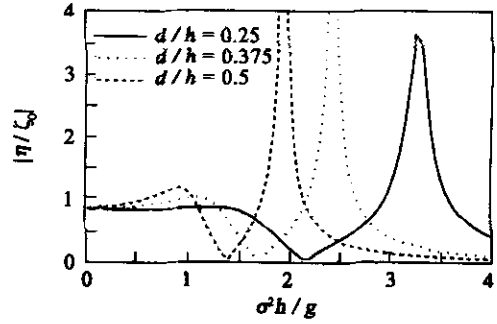

Fig. 13. The influence of pontoon draft on heave motion.
($a/h = d/h = 0.25$; $K/(\rho gh) = 0.05$; $l/h = 0.5$; $\theta = 45°$)

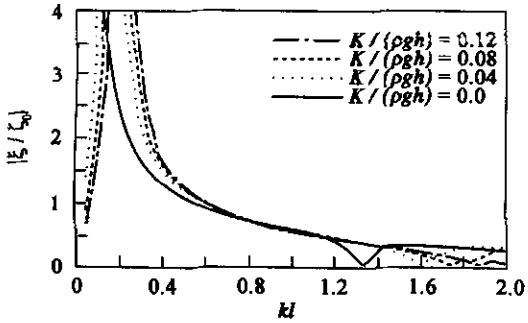

Fig. 14. Effect of stiffness on surge response.

4.4 Influences of Stiffness of Mooring Cable on Structure's Responses

A floating dual pontoon structure with each pontoon width $a = 0.25h$, draft $d = 0.25h$, and space between pontoons $l = 0.5h$, is investigated for understanding the influences of the stiffness of the mooring system on structure's responses. The results are shown in Figs. 14 ~ 16 for four stiffnesses of the mooring lines $K/(\rho gh) = 0.12$, 0.08, 0.04 and 0.0. The angle inclination of each mooring line is kept to $\theta = 60°$ during numerical analysis.

Fig. 14 demonstrates the relationship between the normalized amplitude of surge motion and the parameter kl. As can be seen, the influences of various stiffnesses of the cable are not very obvious for surge motion of the structure. The amplitude of heave motion is described in Fig. 15, and all the results have an identical zero value at the frequency of $kl \approx 1.1$ when the stiffness of the cable changes from 0.0 to 0.12. The overall modulation of heave motion has not large differences from that for a single floating structure, except for the region of $kl \geqslant 1.1$. As can be seen from Fig. 15, the peak re-

sponse of heave in the region $kl \geqslant 1.1$ tends to have higher frequency with the increasing stiffness of the mooring system. Pitch motion as illustrated in Fig. 16, also changes its peak frequency to a higher frequency region when the structure is linked by a cable of larger stiffness.

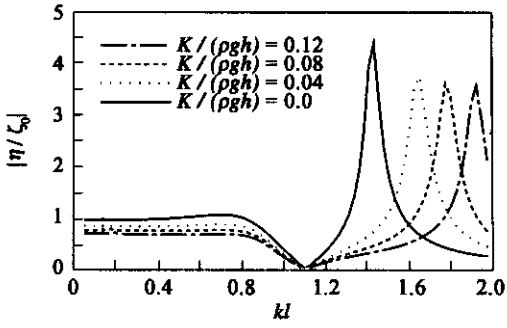

Fig. 15. Effect of stiffness on heave response.

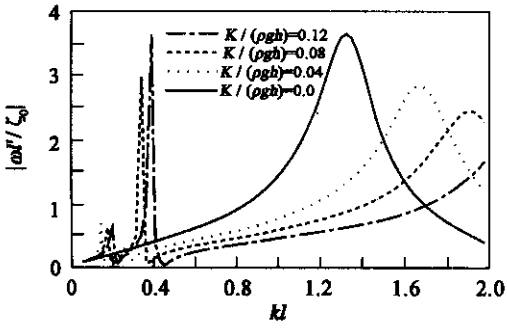

Fig. 16. Effect of stiffness on pitch response.

5. Conclusion

A numerical model has been developed by means of the boundary element method for the analysis of the two-dimensional linearized hydrodynamic problem of a floating dual pontoon structure. Comparisons between numerical results and experimental ones show good agreement for a wide range of parameters, and the validity of this method is therefore confirmed.

The results obtained here indicate that the clear space between pontoons is an important parameter for the behaviors of a floating dual pontoon structure. The clear space has a great effect upon responses of the structure; it not only changes the natural frequency of the structure, but causes heave motion to have a peak response in high frequency range. However, the responses of the floating dual pontoon structure gradually become similar to a single floating body's with the shortening clear distance.

References

Drimer, N., Agnon, Y. and Stiassnie, M., 1992. A simplified analytical model for a floating breakwater in water of finite depth, *Applied Ocean Research*, **14**(1): 33 ~ 41.

Goda, Y. and Suzuki, Y., 1976. Estimation of incident and reflected waves in random wave experiments, *Coastal Engineering*, Vol. 1, ch. 48, 828 ~ 845.

Isaacson, M. and Byres, R., 1988. Floating breakwater response to wave action, *Coastal Engineering*, **162**, 2189 ~ 2200.

Leonard, J. W., Huang, M. C. and Hudspeth, R. T., 1983. Hydrodynamic interference between floating cylinders in oblique seas, *Applied Ocean Research*, **5**(3): 158 ~ 166.

McCartney, B. L., 1985. Floating breakwater design, *Journal of Waterway, Port, Coastal and Ocean Engineering*, ASCE, **111**(2): 304 ~ 317.

McIver, P., 1986. Wave forces on adjacent floating bridges, *Applied Ocean Research*, **8**(2): 67 ~ 75.

Murali, K. and Mani, J. S., 1997. Performance of cage floating breakwater, *Journal of Waterway, Port, Coastal and Ocean Engineering*, ASCE, **123**(4): 172 ~ 179.

Sannasiraj, S. A., Sundar, V. and Sundarvadivelu, R., 1998. Mooring forces and motion responses of pontoon-type

floating breakwaters, *Ocean Engineering*, **25**(1): 27 ~ 48.

WANG Cong, FU shi-xiao, LI Ning, CUI Wei-cheng and LIN Zhu-ming, 2006. Dynamic Analysis of a pontoon-Separated Floating Bridge Subjected to A Moving Load, *China Ocean Eng.*, **20**(3): 419 ~ 430.